Parametric Investigation of the Flight Performance of a Variable Rotor Pitch X-Configuration Quadrotor Aircraft

Dong Han*,

College of Aerospace Engineering, Nanjing University of Aeronautics and Astronautics, Nanjing 210016, China

Linzhen Zhou

College of Aerospace Engineering, Nanjing University of Aeronautics and Astronautics, Nanjing 210016, China

George N. Barakos

CFD Laboratory, School of Engineering, University of Glasgow, G12 8QQ, Scotland, UK

Abstract: To better understand and predict the flight performance of X-configuration quadrotor aircraft using variable **rotor** pitch **and fixed rotor speed** to control the aircraft, a flight performance tool including a rotor model, an aerodynamic interference model and a new propulsive trim method is derived. The lifting rotors are modeled as circular fixed wings, and generate horseshoe vortices trailed from the retreating and advancing sides to affect the aerodynamics of the other rotors. The equilibrium equations of the aircraft are reduced by using symmetry. An iterative method by separately solving for the aircraft pitch and the collective **rotor** pitch is proposed to obtain the converged solution of the reduced equilibrium equations. The aerodynamic interference was found to be beneficial for the front rotors at low to medium speeds, since the nearby front rotors induced a larger upwash than the resultant downwash induced by the rear rotors. The interference is harmful to the rear rotors due to larger downwash induced by the rotors right ahead. The rotors can generate nose up hub pitching moments, which can be used to counter the nose down fuselage pitching moment, and decrease the thrust difference between the front and rear rotors. The effect of the fuselage pitching moment on the rotor power becomes pronounced at medium to high speeds. The vertical distance between the rotor plane and the center of mass of the aircraft can change the pitching

*Corresponding Author, Email Address: donghan@nuaa.edu.cn

moment acting on the aircraft, and its effect is similar to a change in the fuselage pitching moment. Reducing the fuselage drag can lead to larger rotor induced power due to the stronger aerodynamic interference, but the effect is relatively small, and fuselage drag reductions are desirable.

Keywords: Quadrotor Aircraft; X-Configuration; Flight Performance; Aerodynamic Interference; Forward Flight

Nomenclature

C_{M_y}	pitching moment coefficient
D	fuselage drag
e	flap hinge offset
H	rotor drag force
I_β	blade flapping moment of inertia
k	cross-induced velocity factor
k_β	hinge spring stiffness
L_x	longitudinal distance from the rotor shaft to the mass center of the aircraft
L_y	lateral distance from the rotor shaft to the mass center of the aircraft
L_z	vertical distance from the rotor plane to the mass center of the aircraft
M_x	rolling moment
M_y	pitching moment
q	dynamic pressure
Q	rotor torque
R	rotor radius
T	rotor thrust

V_∞	free stream velocity
v_i	induced velocity
w	damping factor
W	weight
Y	rotor side force
α_F	aircraft pitch
γ	wake skew angle
θ_0	collective **rotor** pitch
κ	self-induced velocity factor
ν_β	blade flapping frequency ratio
ρ	air density
Ω	rotor speed
Γ	vortex strength

subscripts

F	contribution from fuselage
1-4	rotor index

1. Introduction

Quadrotor aircraft are multi-rotor helicopters lifted and propelled by four vertically oriented rotors. Before the birth of helicopter, several quadrotor aircraft had been built, for example, the Breguet Gyroplane No. 1 quadrotor, the Jerome-de Bothezat helicopter, and the Ehmichen quadrotor [1]. In recent years, small scale quadrotor aircraft weighting several kilograms have been widely applied in aerial photography, recreation, observation and so on. In

these applications, they don't have to fly very long, fast or high. For applications in transportation, search and rescue, communication, navigation, resource exploration, environment and disaster monitoring and so on, some basic performance requirements, such as payload, endurance, range, maximum forward speed etc., have to be satisfied. To successfully accomplish these missions, large scale quadrotor aircraft are needed. However, current technologies cannot support large high-performance quadrotor aircraft. In comparison to helicopters, electric quadrotors exhibit poor flight endurance attributed to multiple factors such as rotor/motor efficiency and limited battery capacity [2]. To date, most publications on quadrotor aircraft focus on flight dynamics and control [3-10], and fewer concentrate on flight performance, especially for larger scale quadrotor aircraft.

The four equal rotors of the air vehicle provide lift and control forces and moments. According to the location of the rotors, usually there are two configurations: X-configuration (or cross) and +-configuration (or plus). The rotor model is a key part of the quadrotor aircraft model for flight performance prediction. The rotors operate in edgewise (not axial) flight condition, so their aerodynamic characteristics are more like helicopter rotors than propellers, though the flap and lag hinges and the cyclic pitch controls are usually removed from quadrotor systems. Nguyen et al. compared the prediction of the aerodynamic performance of a quadrotor helicopter with experimental data [11]. The rotor model was based on momentum theory and blade element method, while an empirical interference model was used to capture the aerodynamic interaction between the front and rear rotors. The predictions agreed well with experimental data. To compare the performance of a 2-kg quadcopter with variable rotor speed and variable blade pitch, McKay et al. assumed rigid blades and used the blade element theory without the consideration of the aerodynamic interference between the rotors [12]. The difference between the rotor controls indicated that the pitching moments generated by the rotors and the fuselage could have a significant influence on the trim of quadrotor aircraft.

85 An important feature of quadrotor aircraft is that the trailed wakes generated by each rotor can strongly affect the
86 other rotors. Numerical studies of the aerodynamic performance of a quadrotor indicated that the rear rotors were
87 significantly affected by the downwash of the front ones [13], and suggested that including the aerodynamic
88 interactions between the rotors even in the design of the fight control system was recommended. A mathematical
89 model of a quadrotor proposed by Luo et al. considered the aerodynamic interference between rotors at high speed
90 flight, and provided consistent predictions with computational fluid dynamics[14]. Misiorowski et al. calculated the
91 interactional effects for a small scale quadrotor in edgewise flight. For the X-configuration quadcopter, the thrust
92 generated by the rear rotor decreased by 19%, and the torque by 3% due to the aerodynamic interaction at a forward
93 speed of 10m/s [15]. These efforts were limited to a specified flight state (not vehicle trim), or a propulsive trim
94 state without aerodynamic interference between the rotors.
95 In summary, past research focused on the investigation of the flight performance of small scale quadrotor aircraft,
96 and larger designs weighing hundreds or thousands of kilograms were not thoroughly investigated. The literature
97 also indicates that, the pitching moment, aircraft trim, and aerodynamic interference of the rotors may be essential
98 for performance prediction. In addition, the effects of the aircraft trim and pitching moment on the flight
99 performance have not been investigated, but accounting for these in a quadrotor model is a challenging task.
100 In this work, a performance prediction method for a large X-configuration quadrotor aircraft **using variable**
101 **rotor pitch and fixed rotor speed to control the aircraft** is derived. A validated rotor model is applied to the
102 rotors of the quadrotor aircraft [16]. Then, an analytical model to predict the aerodynamic interference between any
103 two rotors of the four is used [17]. A new propulsive trim method considering the forces and moments acting on the
104 rotors and fuselage is also derived. Due to the symmetry of the aircraft configuration, the six equilibrium equations
105 could be reduced to three. An iterative algorithm is proposed to solve the equations and obtain the trimmed flight

106 state. The effects of the aerodynamic interference, pitching moment, location of the mass center, and fuselage drag
107 on the rotor thrusts and power requirements are investigated.

108 **2. Flight Performance Model**

109 The flight performance model of a X-configuration quadrotor primarily consists of a rotor model, a propulsive
110 trim method and an aerodynamic interference model. The equilibrium equations of the X-configuration quadrotor
111 aircraft are based on the forces and moments acting on the rotors and fuselage. An iterative algorithm is proposed to
112 obtain the trimmed solution.

113 **2.1. Rotor Model**

114 The rotor model of the quadrotor aircraft is derived from a helicopter rotor model [16], which consists of a blade
115 structural model, an airfoil aerodynamics model and an induced velocity model. The blade model is based on a
116 rigid beam with a hinge offset and a hinge spring, which is used to match the fundamental flapwise blade frequency.
117 Look-up table airfoil aerodynamics is used to calculate the lift and drag coefficients of blade elements according to
118 the local resultant air flow and angle of attack. The induced velocity over the rotor disk is predicted by the Pitt–
119 Peters inflow model [18], which captures the first harmonic variation of induced velocity in azimuth. The steady
120 responses of blade flapping need to be obtained to get the time histories of the blade root forces and moments with
121 the azimuth, which is used to derive the hub forces and moments. The comparisons of the prediction of the UH-60
122 helicopter rotor power with the flight test data [19] for the takeoff weight coefficients 0.0065 and 0.0074 are shown
123 in Figure 1, which indicates that the predictions by the present method are generally in good agreement with the
124 flight test data for the weights considered. This justifies the use of present method for the analysis of rotor
125 performance. For the application in the rotors of quadrotor aircraft, the cyclic pitch angles are set to be zero.

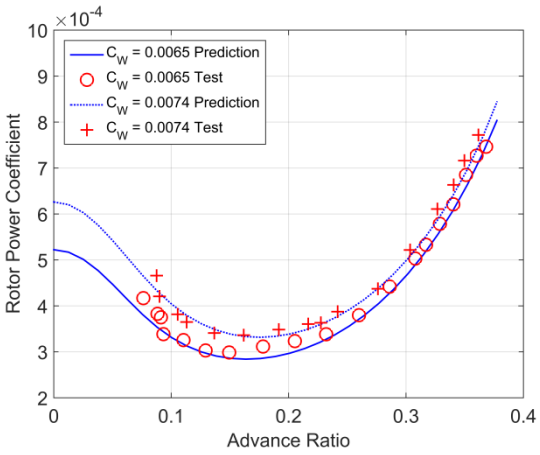

Fig. 1. Comparison of predictions with flight test data from [19].

2.2 Propulsive Trim

For a X-configuration quadrotor, the symmetry about its centerline is usually used, so the side force and the rolling moment acting on the fuselage are zero. With the lift generated by the fuselage omitted, the drag, weight and pitching moment on the fuselage are shown in Figure 2.

Figure 3 shows the rotors of a quadrotor aircraft. The four rotors are named ROTOR 1, ROTOR 2, ROTOR 3, and ROTOR 4. The rotor hub forces and moments, and their corresponding directions are also shown. Due to the different rotation direction, the side forces and rolling moments on ROTOR 1 and ROTOR 4 are different from those acting on ROTOR 2 and ROTOR 3.

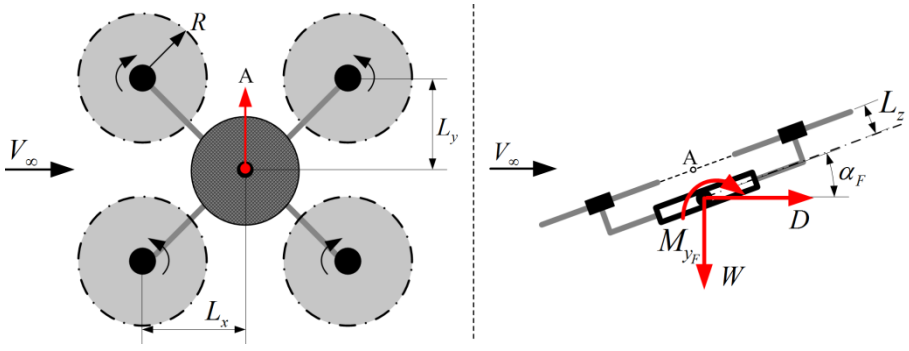

Fig. 2. Forces and moment on the fuselage.

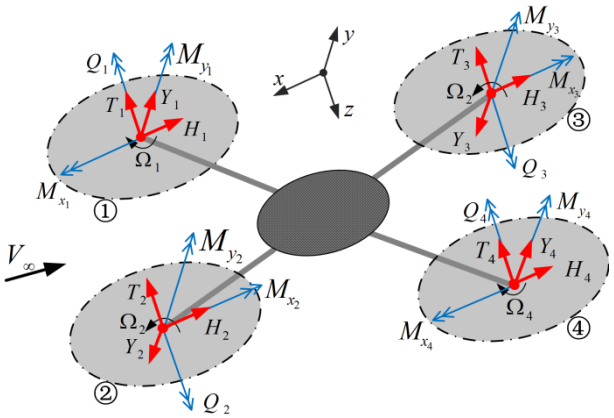

Fig. 3. Forces and moments on the rotors.

Due to the symmetry, the lateral tilt of the aircraft is zero. The weight of the aircraft is balanced by the rotor thrusts and rotor disk-plane forces. In the vertical direction, the forces satisfy:

$$(T_1 + T_2 + T_3 + T_4)\cos\alpha_F + (H_1 + H_2 + H_3 + H_4)\sin\alpha_F = W \tag{1}$$

where, T is the rotor thrust, the subscript 1 to 4 denotes the index of the rotors, H is the rotor drag, α_F is the aircraft pitch, and W is the weight of the aircraft. In the longitudinal direction, the rotor thrusts tilt forward to provide propulsive forces to counteract the fuselage drag, as well as, the components of the rotor drag forces in that direction. This is expressed as:

$$(T_1 + T_2 + T_3 + T_4)\sin\alpha_F - (H_1 + H_2 + H_3 + H_4)\cos\alpha_F = D \tag{2}$$

where, D is the fuselage drag. It is assumed that the action point of the fuselage drag is at the center of mass of the vehicle. The side forces of the rotors Y_i are balanced by themselves, and this relation can be expressed as

$$Y_1 - Y_2 - Y_3 + Y_4 = 0 \tag{3}$$

To simplify the derivation of the equilibrium equation for the pitching moments, the point A (geometric center of

the rotor disks) is designated as the resultant point, as shown in Figure 2. The pitching moments generated by the rotors and the fuselage follow

$$\left(M_{y_1}+M_{y_2}+M_{y_3}+M_{y_4}\right)+(W\sin\alpha_F-D\cos\alpha_F)L_z+M_{y_F}=(T_3+T_4-T_1-T_2)L_x \tag{4}$$

where, M_y is the pitching moment of a rotor hub, M_{y_F} is the pitching moment of the fuselage, L_x is the longitudinal distance from the rotor shaft to the mass center of the aircraft, and L_z is the vertical distance from the rotor plane to the mass center. The rotor rolling moments are balanced by the thrust differences between the left and right rotors about the centerline, which can be expressed as

$$\left(M_{x_1}-M_{x_2}-M_{x_3}+M_{x_4}\right)+(T_1-T_2+T_3-T_4)L_y=0 \tag{5}$$

where, L_y is the lateral distance from the rotor shaft to the mass center of the aircraft. The yawing moments are all generated by the rotors. About point A, the contributions are balanced, following

$$(Y_1-Y_2+Y_3-Y_4)L_x+(H_1-H_2+H_3-H_4)L_y-(Q_1-Q_2-Q_3+Q_4)=0 \tag{6}$$

where, Q is the rotor torque.

Due to the symmetry of the X-configuration quadrotor, the rotor hub forces and moments follow:

$$\begin{cases} T_1=T_2 & Y_1=Y_2 & H_1=H_2 \\ T_3=T_4 & Y_3=Y_4 & H_3=H_4 \end{cases} \tag{7}$$

and

$$\begin{cases} Q_1=Q_2 & M_{x_1}=M_{x_2} & M_{y_1}=M_{y_2} \\ Q_3=Q_4 & M_{x_3}=M_{x_4} & M_{y_3}=M_{y_4} \end{cases} \tag{8}$$

where, Q is the rotor torque, and M_x is the rolling moment of a rotor hub. Combining with Equations 7 and 8, Equations 1, 2 and 4 can be reduced to

$$(T_1 + T_3)\cos\alpha_F + (H_1 + H_3)\sin\alpha_F = \frac{W}{2} \tag{9}$$

$$(T_1 + T_3)\sin\alpha_F - (H_1 + H_3)\cos\alpha_F = \frac{D}{2} \tag{10}$$

and

$$T_3 - T_1 = \frac{\left(M_{y_1} + M_{y_3}\right)}{L_x} + \frac{(W\sin\alpha_F - D\cos\alpha_F)L_z + M_{y_F}}{2L_x} \tag{11}$$

The above three equations can be used to obtain three variables, which are the collective **rotor** pitch angles of ROTORs 1 and 3, i.e. $\theta_0^{(1)}$ and $\theta_0^{(3)}$, and the aircraft pitch α_F. Usually Newton's method is used to solve the nonlinear equations. Since it is hard to give the expression of Jacobi matrix for this problem, the three variables are solved separately and the corresponding iterative algorithms are constructed. Combining Equations 9 and 10, the aircraft pitch becomes

$$\alpha_F = \tan^{-1}\left(\frac{\frac{D}{2} + (H_1 + H_3)\cos\alpha_F}{\frac{W}{2} - (H_1 + H_3)\sin\alpha_F}\right) \tag{12}$$

The following iterative algorithm is proposed to obtain the converged value of the aircraft pitch, which is

$$(\alpha_F)_{n+1} = \tan^{-1}\left(\frac{\frac{D}{2} + [(H_1)_n + (H_3)_n]\cos(\alpha_F)_n}{\frac{W}{2} - [(H_1)_n + (H_3)_n]\sin(\alpha_F)_n}\right) \tag{13}$$

where, the subscript n denotes the value at the n^{th} step. Combining Equations 9 and 11, the rotor thrusts T_1 and T_3

196 can be solved by

197 $$T_1 = \frac{W}{4\cos\alpha_F} - \frac{(H_1 + H_3)\sin\alpha_F}{2\cos\alpha_F} - \frac{\left(M_{y_1} + M_{y_3}\right)}{2L_x} - \frac{(W\sin\alpha_F - D\cos\alpha_F)L_z + M_{y_F}}{4L_x} = T_A$$

198 (14)

199 and

200 $$T_3 = \frac{W}{4\cos\alpha_F} - \frac{(H_1 + H_3)\sin\alpha_F}{2\cos\alpha_F} + \frac{\left(M_{y_1} + M_{y_3}\right)}{2L_x} + \frac{(W\sin\alpha_F - D\cos\alpha_F)L_z + M_{y_F}}{4L_x} = T_B$$

201 (15)

202 To obtain the converged rotor thrusts, Newton's method is used to solve Equations 14 and 15. The iterative

203 equations are

204 $$\left(\theta_0^{(1)}\right)_{n+1} = \left(\theta_0^{(1)}\right)_n - w\left[(T_1)_n - (T_A)_n\right] / \left(\frac{\partial T_1}{\partial \theta_0^{(1)}}\right)_n$$

205 (16)

206 and

207 $$\left(\theta_0^{(3)}\right)_{n+1} = \left(\theta_0^{(3)}\right)_n - w\left[(T_3)_n - (T_B)_n\right] / \left(\frac{\partial T_3}{\partial \theta_0^{(3)}}\right)_n$$

208 (17)

209 where, θ_0 is the collective **rotor** pitch. w is a numerical damping factor to enhance the convergence of the iteration

210 and reduce the computation time, and a value of 0.5 is used here.

211 **2.3 Aerodynamic Interference Model**

212 For predictions of flight performance and for the design of flight control systems of quadrotor aircraft, fast

213 analyses with acceptable precision are required due to design cycle limits and even real-time demands. For the

214 aerodynamic interference models, it is necessary to balance efficiency and accuracy. CFD can provide high

215 precision predictions with a lot of computing resources and time. Currently, it is not practicing to directly use CFD

in the fast prediction of flight performance and in the design of flight control systems. Omitting the aerodynamic interference is also not desirable. In this work, an analytical interference model is used to achieve accuracy and efficient computation.

The theoretical formula on the basis of the Biot-Savart Law is used to predict the aerodynamic interferences among the rotors, which is validated by the experimental results [11]. This method has been extended to consider the aerodynamic interferences for multi-rotors in forward flight [17]. At a forward speed (rotor advanced ratio $\mu > 0.1$), a lifting rotor can be modeled as a circular fixed wing [1, 20]. A horseshoe vortex is trailed from the retreating and advancing sides, as shown in Figure 4. Γ is the strength of the vortex trailed from the tip of the wing. γ is the wake skew angle between the rotor disk and the trailed vortex plane. This aerodynamic interference model assumes that the horseshoe vortex trailed from one rotor generates an additional induced velocity to the other rotor. The velocity in the vertical direction (z direction) at P(x_p, y_p,0) induced by the horseshoe vortex is [17]

$$v_{iP} = \frac{\Gamma \cos\gamma}{4\pi} \cdot \left[\frac{(y_p + R)\left(1 + \frac{x_p \cos\gamma}{\sqrt{x_p^2 + (y_p + R)^2}}\right)}{(y_p + R)^2 + x_p^2 \sin^2\gamma} - \frac{(y_p - R)\left(1 + \frac{x_p \cos\gamma}{\sqrt{x_p^2 + (y_p - R)^2}}\right)}{(y_p - R)^2 + x_p^2 \sin^2\gamma} \right] \tag{18}$$

where, R is the rotor radius. Point P can be considered as the hub center of a rotor. If point P lies between the two vortices and downstream the incoming flow, both vortices induce downwash velocities. If a rotor lies at this location, they can degrade the rotor performance. If point P locates outside the vortices and downstream the incoming flow, the closer vertex induces a larger upwash velocity than the smaller downwash velocity induced by the other further vertex. The resultant velocity at this point is upwash, which reduces the angle of attack of the rotor, and improves the rotor performance.

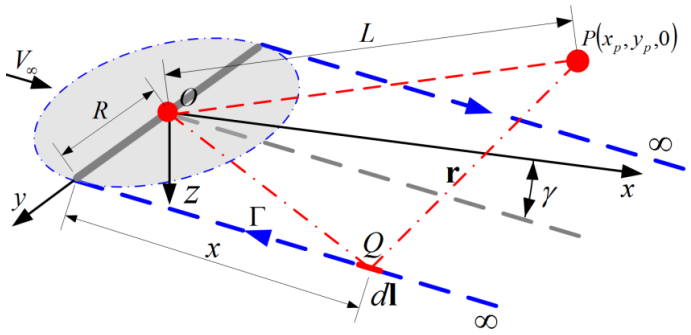

Fig. 4. Coordinate system.

Similar to the method used in Refs. 11 and 20, a dimensionless factor is used to measure the aerodynamic interference. By setting $x_p = y_p = 0$, the induced velocity in the z direction at the center of the rotor disk (point O) is

$$v_{iO} = \frac{\Gamma \cos\gamma}{2\pi R} \tag{19}$$

The non-dimensional expressions of x_p and y_p are defined as

$$\begin{cases} \bar{x}_p = \dfrac{x_p}{R} \\ \bar{y}_p = \dfrac{y_p}{R} \end{cases} \tag{20}$$

The aerodynamic interference factor is defined as the ratio of v_{iP} to v_{iO}, and it can be expressed as

$$k_i = \frac{v_{iP}}{v_{io}} = \frac{1}{2}\left[\frac{(\bar{y}_p+1)\left(1+\dfrac{\bar{x}_p\cos\gamma}{\sqrt{\bar{x}_p^2+(\bar{y}_p+1)^2}}\right)}{(\bar{y}_p+1)^2+\sin^2\gamma\,\bar{x}_p^2} - \frac{(\bar{y}_p-1)\left(1+\dfrac{\bar{x}_p\cos\gamma}{\sqrt{\bar{x}_p^2+(\bar{y}_p-1)^2}}\right)}{(\bar{y}_p-1)^2+\sin^2\gamma\,\bar{x}_p^2}\right] \tag{21}$$

It is assumed that the velocity induced by a rotor on another is uniform. The induced velocity at the rotor hub center can denote the aerodynamic interaction. For a quadrotor, the induced velocity over the rotors can be expressed as

$$\begin{Bmatrix} v_i^{(1)} \\ v_i^{(2)} \\ v_i^{(3)} \\ v_i^{(4)} \end{Bmatrix} = \begin{bmatrix} \kappa_1 & k_{12} & k_{13} & k_{14} \\ k_{21} & \kappa_2 & k_{23} & k_{24} \\ k_{31} & k_{32} & \kappa_3 & k_{34} \\ k_{41} & k_{42} & k_{43} & \kappa_4 \end{bmatrix} \begin{Bmatrix} v_{i0}^{(1)} \\ v_{i0}^{(2)} \\ v_{i0}^{(3)} \\ v_{i0}^{(4)} \end{Bmatrix} \tag{22}$$

where the subscript '0' denotes the velocity of an isolated rotor. k_{ij} denotes the cross-induced velocity factor generated by the *j*th rotor to the *i*th rotor. κ_i is the correction for the self-induced losses of a real rotor.

3. Performance Analysis

This work focuses on the model versatility and fundamental mechanism investigation. For convenience, the rotors of the baseline quadrotor aircraft are the same as the UH-60A rotor without cyclic pitch controls. Currently, no quadrotor aircraft has so large size and heavy weight. It is used as an example aircraft, and may be used for future high-lift aircraft. The parameters of the main rotor are listed in Table 1 [21, 22]. The corresponding distributions of the airfoil and blade pre-twist can be found in Ref. [22]. The aerodynamic fuselage drag equation utilized in the analysis is [18]

$$\frac{D}{q}\,(\mathrm{ft}^2) = 35.83 + 0.016 \times (1.66\alpha_F)^2 \tag{23}$$

where, q is the dynamic pressure. The takeoff weight is assumed to be 4 times the UH-60A helicopter and a weight of 37899kg is used as the baseline. The fuselage drag is also assumed to be 4 times the fuselage drag of UH-60A helicopter shown in Equation 23. The pitching moment coefficient of the fuselage is defined as

$$C_{M_{y_F}} = \frac{M_{y_F}}{\frac{1}{2}\rho V_\infty^2 (\pi R^2)(2L_x)} \tag{24}$$

where, ρ is the air density, and V_∞ is the free stream velocity. For the quadrotor aircraft investigated, L_x and L_y are

both set to be $1.5R$. The quadrotor aircraft flies at sea level.

Table 1 Main rotor parameters [20, 21]

Variable	Value
Main Rotor Radius	8.1778 m
Main Rotor Speed	27.0 rad/s
Blade Chord Length	0.5273 m
Blade Twist	Nonlinear
Blade Airfoil	SC1095/SC1094R8
Number of Blades	4
Flap Hinge Offset	0.381 m
Blade Mass per Unit Length	13.92 kg/m
Longitudinal Shaft Tilt	3°

3.1. Aerodynamic Influence

For convenience, L_z and $C_{M_{y_F}}$ are first set to zero. Figure 5 shows the aircraft pitch with the forward speed, with and without the aerodynamic interference. The aircraft pitch increases with the forward speed, since the fuselage has to tilt more to provide enough propulsive force to balance the increasing drag of the aircraft. The aerodynamic interference causes the increase in the tilt, but the increase is small. At a speed of 250km/h, the aircraft pitch increases by 0.21°. It is obvious that the aerodynamic interference between the rotors has a weak influence on the attitude of the aircraft.

Figure 6 shows the rotor collective **rotor** pitch for different forward speeds with and without the aerodynamic interference. In the figure, Ri denotes rotor i. Without the aerodynamic interference, the difference of the collective **rotor** pitch angles between the front and rear rotors is substantially small. The rear rotor has a larger collective **rotor** pitch than the front rotor within the speed range studied. The collective **rotor** pitch decreases with the forward speed first, and then increases. With the interference considered, the collective **rotor** pitch of the front rotor

decreases at low to medium forward speed, compared with the value without the interference. The interference suggests limited benefits to the front rotor. For the rear rotor, the collective **rotor** pitch increases distinctly, especially at medium speeds, which indicates that the strongest interference occurs at this speed with a strong effect on the rotor performance.

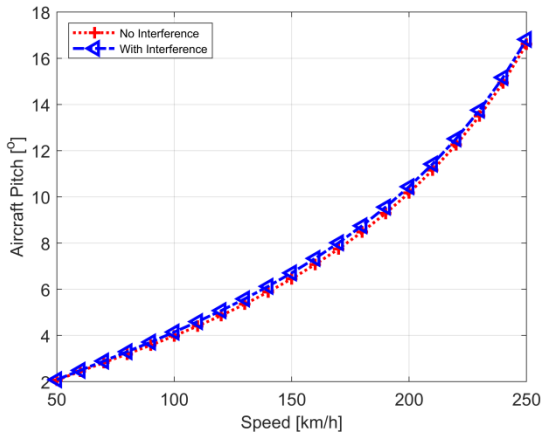

Fig. 5. Aircraft pitch.

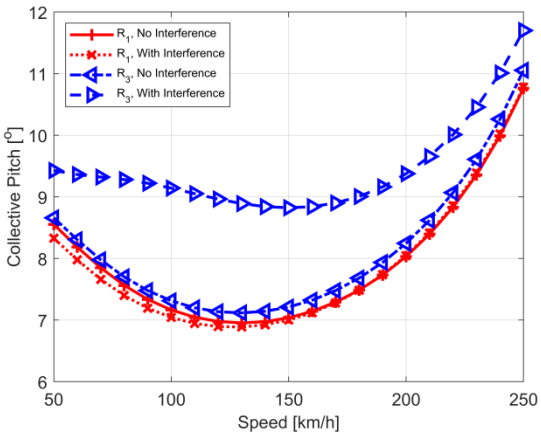

Fig. 6. Collective **rotor** pitch for different forward speed.

Figure 7 shows the variation of the wake skew angle with the forward speed. The skew angles of the front and rear rotors are almost identical. First, they drastically decrease with the forward speed, and then slowly increase. At 160km/h, the minimum occurs. At a low speed, the large induced velocity pushes the trailed wake far from the rotor disk. At a high speed, the aircraft pitch shown in Figure 5 also places the wake far from the rotor disk. The minimum wake skew angle appears at a medium speed, where the strongest aerodynamic interference is seen.

Figure 8 shows the induced factors for different forward speeds. k_{12} is negative, which means the wakes trailed from ROTOR 2 induced a upwash to ROTOR 1. ROTORs 3 and 4 induced downwash to ROTOR 1 but with rather small magnitude. The resultant induced velocity from the other rotors is upwash, which is beneficial for ROTOR 1. k_{31} is much larger than the other factors, which means that the wakes trailed from ROTOR 1 induce a rather large downwash to ROTOR 3. Since the downwash induced by ROTOR 1 is much larger than the resultant upwash induced by ROTORs 2 and 4, especially at medium forward speeds, the performance of ROTOR 3 is

expected to decrease distinctly.

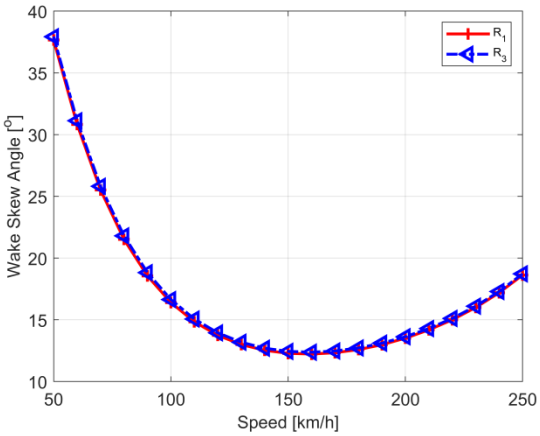

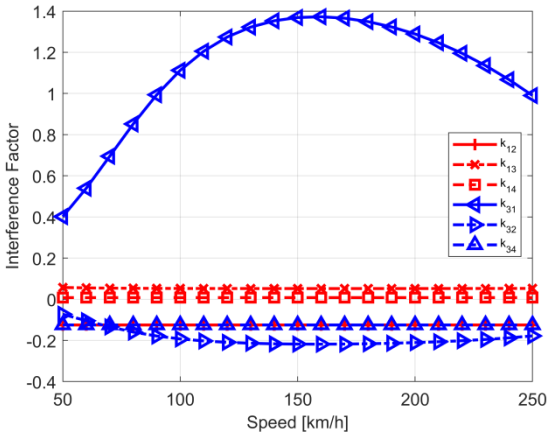

Fig. 7. Wake skew angle for different forward speed. Fig. 8. Induced factors for different forward speed.

Figure 9 shows the rotor thrust for different forward speeds with and without the aerodynamic interference. The interference has a small influence on the rotor thrusts. With an increase in the speed, the rear rotor thrust becomes larger than the front rotor, and the thrust difference increases drastically. At a speed of 250km/h, the difference is 513.2kg without the interference and 528.3kg with it, which has a difference of 2.9%. This thrust difference between the front and rear rotors forms a nose down pitching moment. Since L_z and $C_{M_{y_F}}$ are set to zero, that moment is used to balance the nose up pitching moments generated by the front and rear rotors indicated in Equation 4. Without cyclic pitch controls, the rotors usually generate nose up pitching moments due to the blade flapping, which increase with the forward speed. This is the reason why the trimmed thrust of the rear rotor is larger than the front rotor, and the difference increases with the speed.

Figure 10 shows the rotor power for different forward speeds with and without the aerodynamic interference. Without the interference, the rear rotor consumes more power than the front rotor due to its larger thrust. With the interference, the front rotor power first decreases and then increases by a small amount, compared with the values without the interference. The aerodynamic interference is beneficial for the front rotor at low to medium forward speeds, but the benefit disappears at high speed flight. The rear rotor power increases distinctly, and its performance

reduces significantly. At speeds of 100km/h and 250km/h, the power changes for the front rotor are -2.9% and +0.36%. The values for the rear rotor are +46.1% and +9.4%. The strongest aerodynamic interference on the rear rotor appears at a medium speed due to the wake trailed from ROTOR 1 approaching ROTOR 3 much closer, which is indicated in Figure 8. The power requirement of the whole aircraft increases distinctly. Generally speaking, aerodynamic interference is not beneficial for X-configuration quadrotor aircraft.

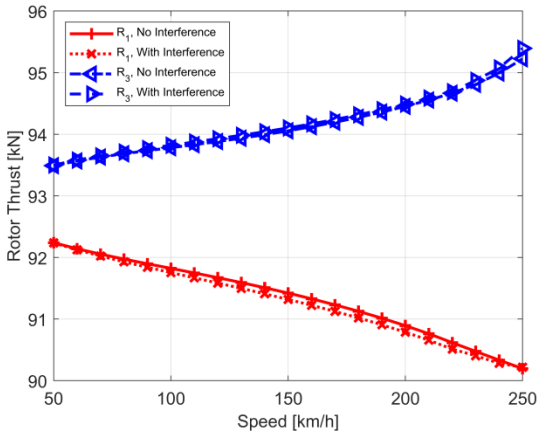

Fig. 9. Rotor thrust for different forward speed.

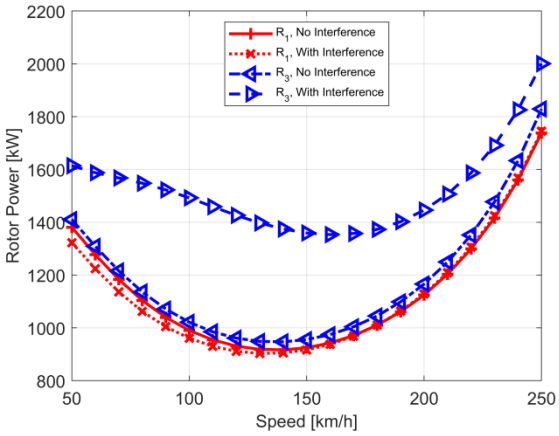

Fig. 10. Rotor power for different forward speed.

The aerodynamic interference primarily changes the induced velocities over nearby rotors, which naturally leads to changes in the induced power. Figure 11 shows the rotor induced power for different forward speeds with and without the aerodynamic interference. The induced power of the front rotor decreases within the speeds studied, when considering the interference. At the speeds of 100km/h and 250km/h, it reduces by 5.5% and 3.9%. For the rear rotor, the interference causes a distinct power increase. The increment first increases with the forward speed, and then decreases. At a medium speed, the increment reaches its maximum. This trend agrees with the variation of the interference factor shown in Figure 8.

Figure 12 shows the rotor profile power for different forward speed with and without the aerodynamic interference. For the front rotor, the change in the profile power is little. For the rear rotor, the increase is obvious, but the magnitude is relatively small compared with the induced power. At a speed of 250km/h, the change of the

profile power of the rear rotor is 7.6% of the total rotor power change. The increment of the induced power contributes most of the power increase seen in the rear rotor.

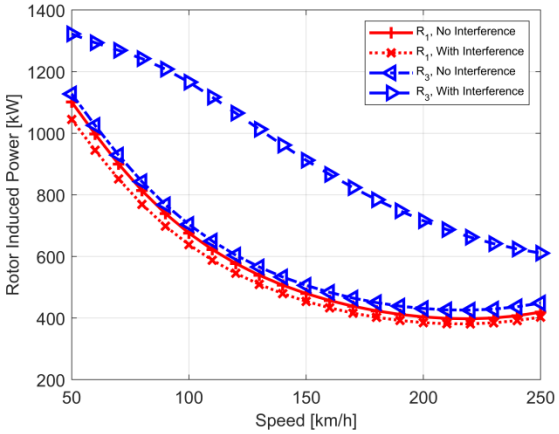

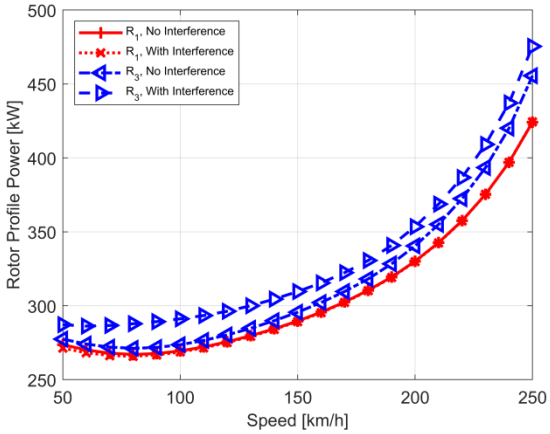

Fig. 11. Rotor induced power for different forward speed. Fig. 12. Rotor profile power for different forward speed.

It should be pointed out that, the front rotor power increases with a very small magnitude at high speed flight due to the aerodynamic interference. At this state, the induced power decreases and the profile power remains unchanged. However, the tilt of the aircraft increases, as shown in Figure 5, which increases the drag of the aircraft. The front rotor has to generate a larger propulsive force, and the parasitic power increases correspondingly. The increase in the parasitic power counteracts the decrease in the induced power.

3.2 Fuselage Pitching Moment

The previous results indicate that each rotor typically produces a pitching up moment and the difference of thrust between front and rear rotors balances it. Usually, aircraft fuselages generate nose down pitching moments. To investigate the effect of the pitching moment of the fuselage on the trim and flight performance, the pitching moment coefficient of the quadrotor aircraft is set to -0.01, -0.02 or -0.03.

Figure 13 shows the aircraft pitch with the forward speed for different fuselage pitching moment. The aircraft pitch angles are almost identical, which suggests that the pitching moment has little influence on the tilt of the fuselage. Equation 12 illustrates that the aircraft pitch is primarily determined by the forces acting on the aircraft,

and the moment has little influence.

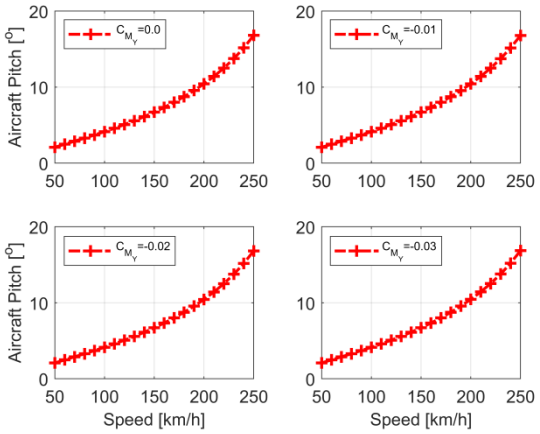

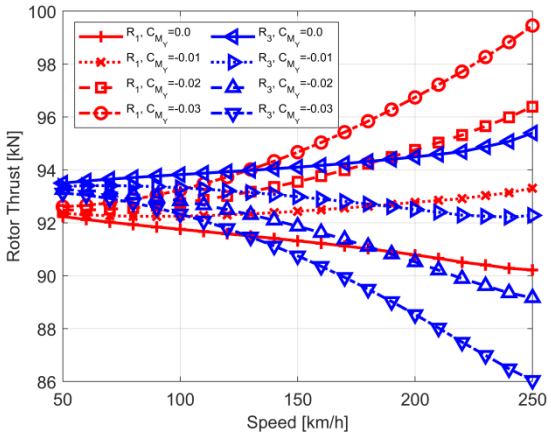

Fig. 13. Aircraft pitch for different pitching moment. Fig. 14. Rotor thrust for different pitching moment.

Figure 14 shows the rotor thrust with the forward speed for different fuselage pitching moment. At a low speed, the rear rotor generates a larger thrust than the front, since the sum of the nose up pitching moments generated by the rotors is larger than the nose down moment generated by the fuselage. Otherwise, the rear rotor generates smaller thrust. At a larger pitching moment coefficient and faster forward speed, the front rotor generates larger thrust. At a speed of 250km/h and moment coefficient of -0.03, the front rotor generates 1368.3kg more thrust than the rear rotor. Large pitching moments can cause large thrust differences between the front and rear rotors, which may not be desirable, especially if simple and economic designs of quadrotors employ similar rotors front and back. The pitching moment mainly changes the rotor thrusts, not the attitude of the rotor disk, and has little influence on the wake skew angles. It can be deduced that the pitching moment has little influence on the aerodynamic interference.

Stiffer rotors can provide larger rotor rolling and pitching moments. To counteract the nose down pitching moment generated by the fuselage, an effective means is to make the blades stiffer in the flapwise direction, which agrees with the increase in the natural frequency of the fundamental flapping mode. For an articulated rotor with uniform blade properties, the blade flapping frequency ratio can be calculated by

$$\nu_\beta = \sqrt{1 + \frac{3e}{2R} + \frac{k_\beta}{I_\beta \Omega^2}} \tag{25}$$

where, e is the flap hinge offset, k_β is the hinge spring stiffness, I_β is the blade flapping moment of inertia, and Ω is the rotor speed.

For the baseline blade used in this work (articulated, $k_\beta = 0$), the frequency ratio is 1.034. By adding a suitable hinge spring, the frequency ratio can be increased. The pitching moment of the fuselage is set to -0.03. Figure 15 shows the thrust difference (the front rotor thrust minus the rear rotor thrust) with the forward speed, for different blade flapping frequency ratios. For the baseline rotor with a frequency ratio of 1.034, the front rotor generates much larger thrust than the rear rotor at medium to high speed flight. This nose up moment due to thrust unbalance decreases distinctly with increasing frequency ratio. It can thus be concluded that using stiffer blades can effectively produce nose up pitching moment to balance the nose down pitching moment generated by the fuselage. This can be helpful to reduce the thrust difference between the front and rear rotors.

Figure 16 shows the rotor power with the forward speed for different fuselage pitching moment. The pitching moment has substantially small influence on the front and rear rotor power, and the effect becomes pronounced at large forward speeds. At very high speeds, the variation of power is noticeable. As the pitching moment changes from 0.0 to -0.03, the front rotor power increases by 10.4% and the rear rotor power decreases by 8.4% at a speed of 250 km/h. The total power increases by 0.26%, which is a very small change. Due to the increase in one rotor power with the decrease in the other rotor, the change of the overall power is relatively small. The pitching moment changes the power distribution between the front and rear rotors, but not the total power.

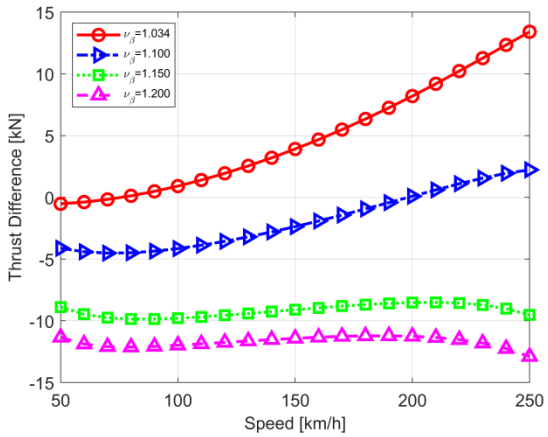

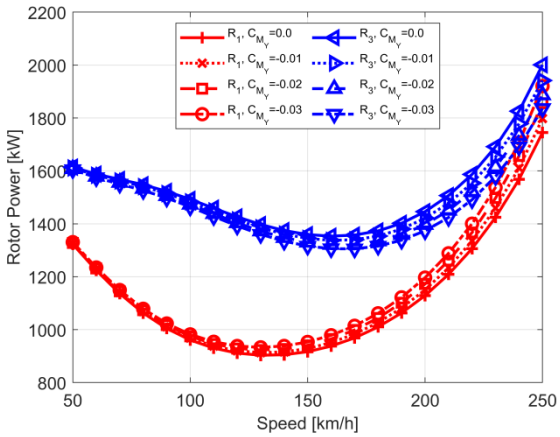

Fig. 15. Thrust difference for different flapping frequency. Fig. 16. Rotor power for different pitching moment.

3.3 Vertical Distance between the Rotor Plane and Mass Center

To investigate the effect of the vertical distance between the rotor plane and the mass center of the aircraft, the pitching moment of the aircraft is set to zero. Figure 17 shows the rotor thrust with the forward speed for different vertical distances of -0.2R, 0.0R and 0.2R. Different vertical distances lead to different distributions of the rotor thrusts between the front and rear rotors. In the three cases studied, the rear rotor generates larger thrust than the front rotor, which can lead to a nose down pitching moment. Changing the location of the mass center relative to the rotor plane changes the pitching moments generated by the fuselage drag and aircraft weight about the geometrical center indicated in Equation 4. Its effect is similar to changing the pitching moment of the fuselage. Lowering the mass center leads to a larger nose up pitching moment to be balanced. Raising the mass center, the moment decreases. It can be concluded that the thrust difference can be adjusted or optimized by changing the position of the mass center relative to the rotor plane. Since the vertical distance changes the pitching moment, its effect is similar to changing the pitching moment of the fuselage.

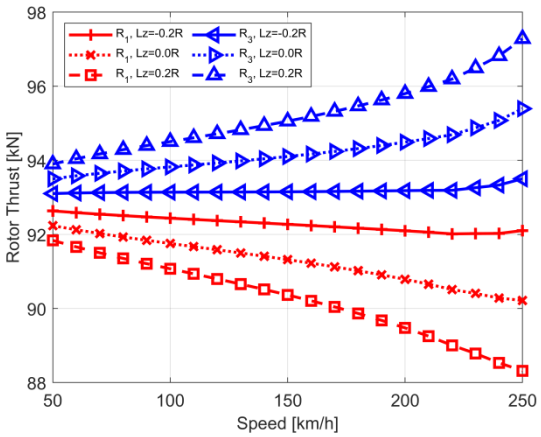

Fig. 17. Rotor thrust for different vertical distance.

The position of the mass center relative to the rotor plane has substantially small influence on the rotor power. At a speed of 250km/h, raising the mass center above the rotor plane by 0.2R leads to an increase in the front rotor power by 1.8%, and a decrease in the rear rotor by 1.8%. Lowering the center below by 0.2R leads to a decrease in the front rotor power by 1.7%, while the rear rotor power increases by 2.0%. The total power of the aircraft remains almost unchanged.

3.4 Fuselage Drag

The pitching moment of the fuselage and the vertical distance between the rotor plane and the mass center are set to zero. Figure 18 shows the aircraft pitch with the forward speed for different fuselage drag values (reducing the drag to 25%, 50% and 75% of the baseline). It is obvious that the aircraft pitch increases drastically with the speed, especially at high speed flight, which is due to the fast increase in the drag with the aircraft pitch. Reducing the drag decreases the aircraft pitch, since smaller propulsive force is needed to balance the drag.

Figure 19 shows the rotor thrust with the forward speed for different fuselage drags. The rotor thrust changes substantially small with the forward speed, even at a high speed. At a speed of 250km/h, the rear rotor thrust decreases by 0.84%, and the front rotor thrust increases by 0.18%, as the fuselage drag decreases by 50%. Larger fuselage drag leads to larger aircraft pitch, as shown in Figure 18, since the rotors have to generate more propulsive

force.

Figure 20 shows the rotor power with the forward speed for different fuselage drag values. At low to medium speed flight, the variation of the front or rear rotor power is relatively small. At a high speed, the front or rear rotor power decreases distinctly with the reduction of the fuselage drag, which means the reduction of the parasitic power of the aircraft. Naturally, the rotor power decreases. At a speed of 150km/h, as the fuselage drag decreases by 50%, the front rotor power decreases by 9.2%, and the rear rotor power decreases by 4.0%. At a speed of 250km/h, the values for the front and rear rotors are 30.6% and 26.8%. Reducing the fuselage drag at high speed flight is seen to be highly beneficial.

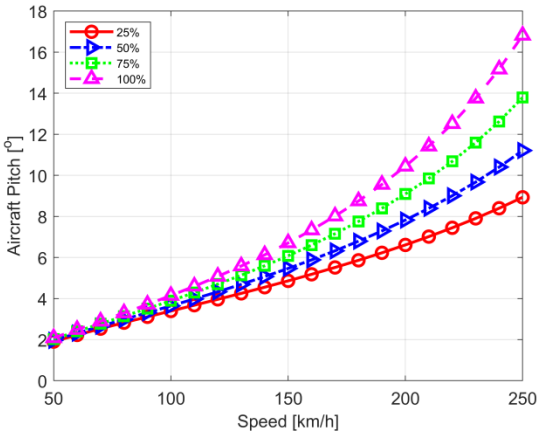

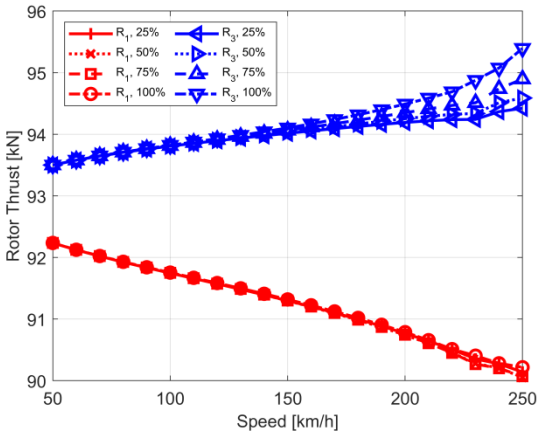

Fig. 18. Aircraft pitch for different fuselage drags. Fig. 19. Rotor thrust for different fuselage drags.

Figure 21 shows the rotor induced power with the forward speed for different fuselage drags. For the front rotor, the variation of the induced power is rather small. For the rear rotor, the induced power increases with the decrease in the drag. At a speed of 250km/h, the induced power of the rear rotor increases by 13.7% with the drag decreasing by 75%, but the magnitude is much smaller than the change of the rotor power. The aircraft pitch decreases with reducing the drag, as show in Figure 18. The decrease in the aircraft pitch can lead to the increase in the aerodynamic interference, which can cause the increase in the induced power of the rear rotor.

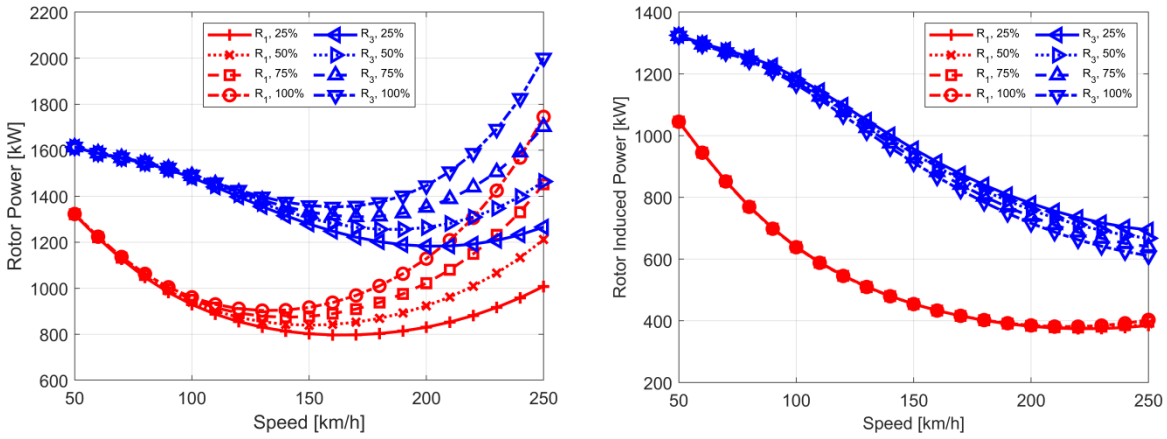

Fig. 20. Rotor power for different fuselage drags. Fig. 21. Rotor induced power for different fuselage drags.

Figures 22 and 23 show the interference factors with the forward speed for different fuselage drags. k_{12} and k_{14} remain almost unchanged with the drag. k_{13} decreases with the decrease in the drag, especially at a high speed. However, the magnitude is rather small. So, the aerodynamic interference between the rotors has little effect on the induced power of the front rotor, as the fuselage drag changes. k_{31} increases, as the drag decreases. It dominates the aerodynamic interference on the rear rotor, and causes an increase in the induced power. The variation of k_{32} indicates that the positive effect increases, as the drag decreases. However, the magnitude is small compared with k_{31}. k_{34} remains unchanged with the drag. As the fuselage drag decreases, the aircraft pitch also decreases. The wake trailed from the front rotor approaches the rear rotor, and then the induced power of the rear rotor increases.

Figure 24 shows the rotor profile power with the forward speed for different fuselage drags. Reducing the drag can decrease the rotor profile power, especially at high speed flight. At a speed of 250km/h, the profile power of the front rotor decreases by 5.2%, as the drag is reduced by 50%. This value is 11.8% for the rear rotor. The absolute change of the profile power is much small compared with the change of the rotor power shown in Figure 20. The change of the profile power of rear rotor is 10.4% of the change of the rotor power. It can be concluded that the reduction of the power is mainly due to the reduction of the parasitic drag.

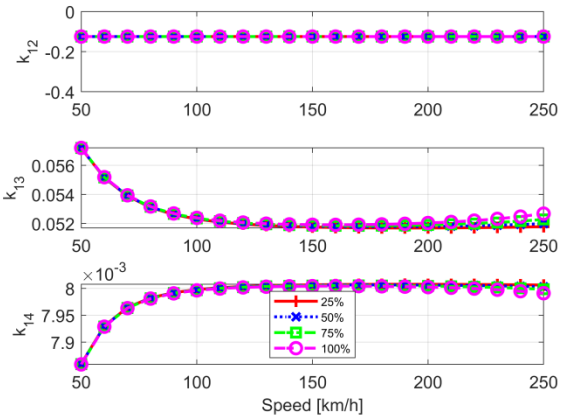

Fig. 22. Interference factors to ROTOR1 .

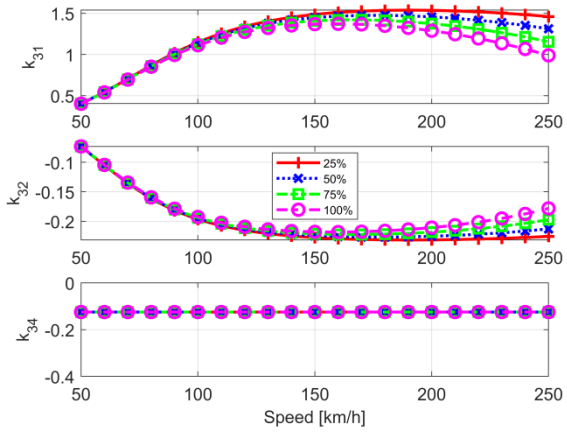

Fig. 23. Interference factors to ROTOR 3.

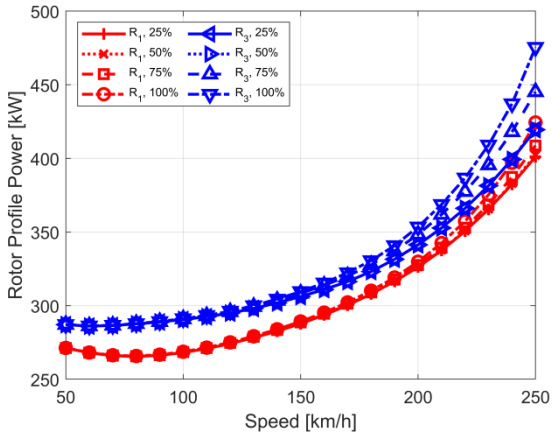

Fig. 24. Rotor profile power with forward speed for different fuselage drag values.

4. Conclusions

To analyze the flight performance of a X-configuration quadrotor, a performance model considering the propulsive trim of the whole aircraft combined with an aerodynamic interference model among the four rotors is derived. By using the configuration symmetry of the quadrotor aircraft, the six equilibrium equations is reduced to three. An iterative algorithm is proposed to obtain the converged solution of the equations. The analyses yielded the following conclusions:

1) The aerodynamic interference is beneficial for the front rotors at low to medium speed flight, since the nearby front rotor mutually induced a larger upwash than the resultant downwash induced by the rear rotors. The collective

463 **rotor** pitch and power of the front rotor decrease with a small magnitude, and this benefit disappears at high speed
464 flight.

465 2) The aerodynamic interference is harmful to the rear rotors, since the front rotor right ahead a rear rotor induces
466 a rather larger downwash than the resultant upwash induced by the two side rotors. The collective **rotor** pitch and
467 power increase distinctly. This side effect culminates at a medium speed.

468 3) The rotors can generate nose up pitching moments, which can cause the thrust generated by the rear rotor is
469 larger than the front rotor. The thrust difference increases distinctly with increasing the forward speed. This nose up
470 pitching moment can be increased by increasing the blade rigidity in the flapwise direction, which can be used to
471 counteract the pitching moment generated by the fuselage to reduce the thrust difference.

472 4) The pitching moment of the fuselage primarily changes the rotor collective angles and the thrust distribution
473 between the front and rear rotors. It has a very small influence on the aircraft pitch, and is not significantly affected
474 by the aerodynamic interference. It can, however, affect the rotor power, and this becomes pronounced at medium
475 to high speed flight.

476 5) The vertical distance between the mass center of the quadrotor aircraft and the rotor plane primarily changes
477 the distribution of the thrusts between the front and rear rotors, and has substantially small effect on the rotor
478 powers. Since the vertical distance changes the pitching moment, its effect is similar to changing the pitching
479 moment of the fuselage.

480 6) Reducing the fuselage drag may lead to an increase in the rotor induced power, due to the stronger
481 aerodynamic interference. However, the magnitude of this increase is small. Reducing the fuselage drag can lead to
482 a small reduction of the rotor profile power. Its reduction comes from the decrease in the parasite power.

483 **Data Availability Statement**

Some or all data, models, or code that support the findings of this study are available from the corresponding author upon reasonable request.

Acknowledgments

This work is supported from the National Natural Science Foundation of China (11972181), the Six Talent Peaks Project in Jiangsu Province (GDZB-013), and the Open Research Foundation of the Key Rotor Aerodynamics Laboratory (RAL20200104).

References

1. Leishman J G. Principles of Helicopter Aerodynamics, 2nd ed., Cambridge Univ. Press, Cambridge, New York, USA, 2006.
2. Winslow J, Benedict M, Hrishikeshavan V, Chopra I. Design, Development, and Flight Testing of a High Endurance Micro Quadrotor Helicopter, International Journal of Micro Air Vehicles 2016; 8(3): 155-169.
3. Modirrousta A, Khodabandeh M. A Novel Nonlinear Hybrid Controller Design for an Uncertain Quadrotor with Disturbances, Aerospace Science and Technology 2015; 45: 294-308.
4. Niemiec R, Gandhi F. Multirotor Controls, Trim, and Autonomous Flight Dynamics of Plus- and Cross-Quadcopters, Journal of Aircraft 2017; 54(5): 1910-1920.
5. Wang R, Liu J. Adaptive formation control of quadrotor unmanned aerial vehicles with bounded control thrust, Chinese Journal of Aeronautics 2017, 30(2): 807-817.
6. Miranda-Colorado R, Aguilar L T, Herrero-Brito, J E. Reduction of Power Consumption on Quadrotor Vehicles via Trajectory Design and a Controller-Gains Tuning Stage, Aerospace Science and Technology 2018; 78: 280-296.
7. Bouzid Y, Siguerdidjane H, Bestaoui Y. Energy based 3D trajectory tracking control of quadrotors with

505 model-free based on-line disturbance compensation, Chinese Journal of Aeronautics 2018, 31(7): 1568-
506 1578.
507 8. Alabsi M I, Fields T D. Real-Time Closed-Loop System Identification of a Quadcopter, Journal of Aircraft
508 2019, 56(1): 324-335.
509 9. Sun S, de Visser C C, Chu Q. Quadrotor Gray-Box Model Identification from High-Speed Flight Data,
510 Journal of Aircraft 2019, 56(2): 645-661.
511 10. Zhang W, Dong C, Ran M, Liu Y. Fully distributed time-varying formation tracking control for multiple
512 quadrotor vehicles via finite-time convergent extended state observer, Chinese Journal of Aeronautics
513 2020, 33(11): 2907-2920.
514 11. Nguyen D H, Liu Y, Mori K. Experimental Study for Aerodynamic Performance of Quadrotor Helicopter,
515 Tans. Japan Soc. 2018; 61(2): 29-39.
516 12. McKay M E, Niemiec R, Gandhi F. Performance Comparison of Quadcopters with variable-RPM and
517 Variable-Pitch Rotors, Journal of the American Helicopter Society 2019; 64(4): 0420061-04200614.
518 13. Hwang J Y, Jung M K, Kwon O J. Numerical Study of Aerodynamic Performance of a Multirotor
519 Unmanned-Aerial-Vehicle Configuration, Journal of Aircraft 2015; 52(3): 839-846.
520 14. Luo J, Zhu L, Yan G. Novel Quadrotor Forward-Flight Model Based on Wake Interference, AIAA Journal
521 2015; 53(12): 3522-3533.
522 15. Misiorowski M, Gandhi F, Oberai A A. Computational Study on Rotor Interactional Effects for a
523 Quadcopter in Edgewise Flight, AIAA Journal 2019; 57(12): 5309-5319.
524 16. Han D, Dong C, Barakos G N. Performance Improvement of Variable Speed Rotors by Gurney Flaps,
525 Aerospace Science and Technology 2018; 81: 118-127.

17. Han D, Barakos G N. Aerodynamic Interference Model for Multi-Rotors in Forward Flight, Journal of Aircraft 2020; 57(6): 1220-1223.

18. Peters D A, HaQuang N. Dynamic Inflow for Practical Application, Journal of the American Helicopter Society 1988; 33(4): 64-68.

19. Yeo H, Bousman W G, Johnson W. Performance Analysis of a Utility Helicopter with Standard and Advanced Rotors, Journal of the American Helicopter Society 2004; 49(3): 250-270.

20. McCormick B W. Aerodynamics of V/STOL Flight, Academic Press Inc., New York, USA, 1967, pp. 148-152.

21. Hilbert K B. A Mathematical Model of the UH-60 Helicopter, Technical Report NASA-TM-85890, 1984.

22. Davis S J. Predesign Study for a Modern 4-Bladed Rotor for the RSRA, Technical Report NASA-CR-166155, 1981.